
Proceedings Paper:
Balasubramanian, L., Wray, T. and Damian, D.D. orcid.org/0000-0002-0595-0182 (2020) Fault tolerant control in shape-changing internal robots. In: Proceedings of 2020 IEEE International Conference on Robotics and Automation (ICRA). 2020 IEEE International Conference on Robotics and Automation (ICRA), 31 May - 31 Aug 2020, Paris, France. IEEE , pp. 5502-5508. ISBN 9781728173962

https://doi.org/10.1109/ICRA40945.2020.9196989

Fault Tolerant Control in Shape-Changing Internal Robots

Lavanya Balasubramanian[1], Tom Wray[1], and Dana D. Damian[1]

***Abstract*— It is known that the interior of the human body is one of the most adverse environments for a foreign body, such as an *in-vivo* robot, and vice-versa. As robots operating *in-vivo* are increasingly recognized for their capabilities and potential for improved therapies, it is important to ensure their safety, especially for long term treatments when little supervision can be provided. We introduce an implantable robot that is flexible, extendable and symmetric, thus changing shape and size. This design allows the implementation of an effective fault tolerant control, with features such as physical polling for fault diagnosis, retraction and redundancy-based control switching at fault. We demonstrate the fault-tolerant capabilities for an implantable robot that elongates tubular tissues by applying tension to the tissue. In benchtop tests, we show a reduction of the fault risks by at least 83%. The study provides a valuable methodology to enhance safety and efficacy of implantable and surgical robots, and thus to accelerate their adoption.**

I. Introduction

Tissue regeneration and growth are lengthy and physiologically demanding processes [1]. There are innumerable cases in which the regenerative capability of the human body cannot carry out these processes without assistance. For instance, long-gap esophageal atresia (LGEA) (Fig. 1) and short bowel syndrome (SBS) are congenital defects in which up to two thirds of the organ (esophagus and bowel respectively) are missing.

Current treatments suggest that mechanical stimulation of the esophagus and bowel has the potential to lengthen these organs [2], [3]. However further efforts are needed in order to reduce the morbidity of these treatments, due to the invasiveness of the underlying surgical intervention, the ad hoc provision of mechanical stimulation, and the necessary post-surgical treatment. It would be ideal to have a robotic implant that resides inside the body, mounted on the esophagus or bowel, and provides precise, localized and effective mechanical stimulation until these tubular organs are fully reconstructed.

Implantable technologies that can operate in the long term inside the body and provide onboard clinical expertise until the tissue heals can facilitate long-term therapies. Such robotic implantable devices not only could complement a surgeon's capabilities but also deliver effective therapy at all times during treatment through their ability to operate autonomously [4], which is impossible in typical forms of clinical practice. Robotic implantable technology also has the potential to adjust and customize treatments, depending on the target tissue and patient state. Lastly, treatment costs can be dramatically reduced, as part of the treatment can be carried out at home.

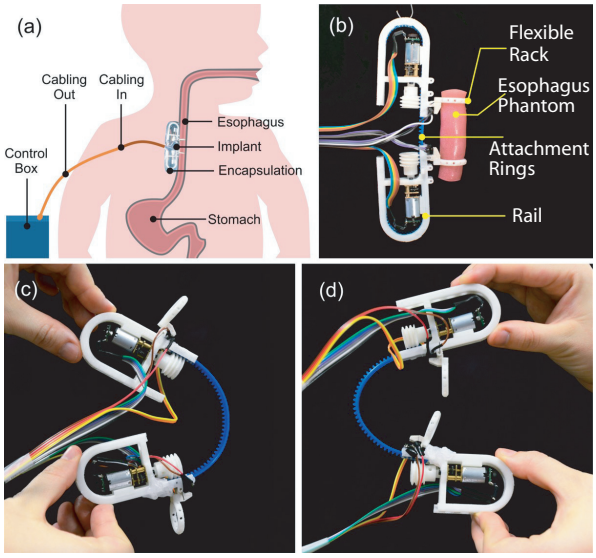

Fig. 1. Overview of the shape-changing implantable robot. (a) Illustration of the robot attached to the esophagus of a baby with esophageal atresia, (b) Key components of the robot, (c,d) Shape and size variation of the robot due to rack's flexion and extension.

While robotic implantable devices can bring significant treatment outcomes, clinical challenges associated with their long-term use do exist. The interior of the human body is one of the most adverse environments for a foreign body, especially for implantable technology. Foreign bodies, including any implant, generate inflammation and scarring that reduce treatment effectiveness. Furthermore, evidence suggests [5] that an inflammatory reaction to a foreign body is exacerbated when an implant is stiffer than the natural tissues in its proximity. These implantable devices may also pose safety risks in case of device breakage. The design of any robotic implantable device must take all these challenges into account. This work addresses these challenges by developing a shape-changing implantable robot (SIR). The SIR is flexible and extendable and has a symmetric functional structure. These features jointly allow SIR to conform to surrounding tissues and thus possibly induce less scarring, and implement active behaviors to poll and resolve faults to improve its resilience and extends its lifespan.

The contributions of this work are: (1) introduction of the concept of fault tolerance in robots that change shape and size (i.e., flexible and extendable) with direct relevance to implantable technologies; (2) design of a shape-changing robot for use as an implant for tissue regeneration; (3)

[1] Automatic Control and Systems Engineering Department, University of Sheffield, Mappin Street, S13JD, UK (e-mail: d.damian@sheffield.ac.uk).

This work was supported by The University of Sheffield and EPSRC R/150439.

introduction of active fault detection, retraction, recovery and redundancy-based compensation strategies based on the shape and structural reconfigurability of the robot; (4) demonstration of the benefit of robot flexibility for fault tolerance, such as disambiguation in fault identification.

II. Related Work

In recent years, we have seen a recognition of the need for and potential of flexible and soft technologies to be used in safe and conformable medical devices. These developments range from smart materials for stents to novel implantable sensors and actuators. Stents made of nitinol exhibit self-expansion due to mechanisms of shape memory and superelasticity [6]. Xu *et al*. developed a soft membrane equipped with arrays of multi-functional sensors and electronic and optoelectronic components that can be placed around the heart to acquire physiological information about the heart's function [7]. Roche *et al*. developed a soft sleeve to support heart function by activating embedded pneumatic actuators that can act as a bridge to transplant for patients with heart failure [8]. A smart ingestible robot that can unfold in the stomach can act as a therapeutic patch for peptic ulcers [9].

Our group has recently developed a robotic implant for esophageal tissue growth with applications for LGEA [10], [11]. The robot, attached to the tissue with two rings, mimics the Foker technique by gently pulling on the tissue using a direct current (DC) motor. We demonstrated *in-vivo* that we can monitor and command these elongation forces and induce cell proliferation in a swine model [12].

While the potential of *in-vivo* robots is recognized, clinical acceptance is hindered by the susceptibility to failure of complex medical devices. Therefore, safety is a key requirement for any clinical translation of the robotic implant [13]. The advancement of *in-vivo* robots will have to be aligned with the development of fault-tolerant systems that will extend their operational life in case of any fault occurrence [14].

Fault-tolerant mechanisms and control have been extensively used in aeronautics; yet fault tolerance and long-term operation have been of increased interest in robotics [15], with researchers exploring robotic body-image [16], soft encapsulation [17], and trial-and-error learning to increase the resilience of robots to fault [18]. Fault-tolerant mechanisms and control have yet to be adopted for medical robots. As *in-vivo* robots operate in inaccessible sites over an extended period of time with limited supervision, a fault tolerance strategy is necessary to detect and compensate for any faults [19].

In this work, we advance our robotic implant technology with shape-changing design features which we show to enhance fault tolerant control.

III. Implant Requirements and Design

A. Requirements

Our *in-vivo* studies [12] have revealed unrecognized challenges owing to the fixed design of the implant operating over the long term in a harsh *in-vivo* environment. Aside from the conventional requirements for implantable technologies, such as biocompatibility, safety, additional stringent requirements need to be met.

The physical requirements are as follows:

a) Implant flexibility: The robotic implant must be mechanically compliant (e.g., flexible) with the surrounding soft tissue. We have ascertained in our previous work that tissue fibrosis occurred at a notable level due to the contact forces between the rigid implant and tissue [12]. A flexible robotic implant should inflict minimum damage to the surrounding organs and minimize fibrotic response [5].

b) Encapsulation: A soft, liquid-proof and airtight cover for the implant to prevent damage to itself and its surrounding organs.

c) Hardware redundancy: In order to reduce surgical intervention, hardware redundancy would prove vital in case of component failure.

The functional requirements are as follows:

d) Tissue tensioning and elongation: As a specific requirement based on our previous work, the robotic implant must be capable of applying a tension force to the tissue of up to $2\,\mathrm{N}$. The robot also needs to provide sufficient tissue displacement capability, approximately $100\,\mathrm{mm}$ [2].

e) Implant fault tolerance: The robotic implant should also be resilient to fault in order to guarantee its long-term use, which can range from weeks to months of treatment. From our experiments, the electronic parts were the components that were most prone to failure. A mechanism and control should be available for the robot to diagnose and compensate for any faults, thus extending its operational life and avoiding re-operative surgery. The focus of this study is on the hardware redundancy and the implant fault tolerance. The other requirements are detailed in a different investigation of our group [20].

B. Implant Design

Based on the above design requirements, we advanced our robotic implant [12] to a flexible, extendable and symmetric design (Fig. 1 (b)(c)(d)), which provide enhanced fault tolerant control (FTC), as demonstrated in the following sections.

A flexible rack was used to ensure that the implant would comply with the dynamics of the surrounding tissue to avoid applying excessive stress to the organs in its proximity, as well as reduce self-damage due to long-term shear stresses. The width of the rack is $8\,\mathrm{mm}$, the total height is $3.8\,\mathrm{mm}$, the width and height of the teeth is 3.8 and $1.8\,\mathrm{mm}$, respectively. Two identical U-shaped rails, also referred to as the main and mirror units, guide the rack displacement and house the required electronics. The U-shape of the rail enables housing an extra length of rack while reducing the overall length of the robotic implant. The dimensions of the rail are as follows: height = $67.35\,\mathrm{mm}$, width = $38.51\,\mathrm{mm}$, and depth = $15.30\,\mathrm{mm}$. The overall length of the robot is $135\,\mathrm{mm}$ (when the two rails are in contact), and the width is $35\,\mathrm{mm}$; these dimensions are 35% and 16% larger than their respective counterparts in [12]. The weight of this core prototype is

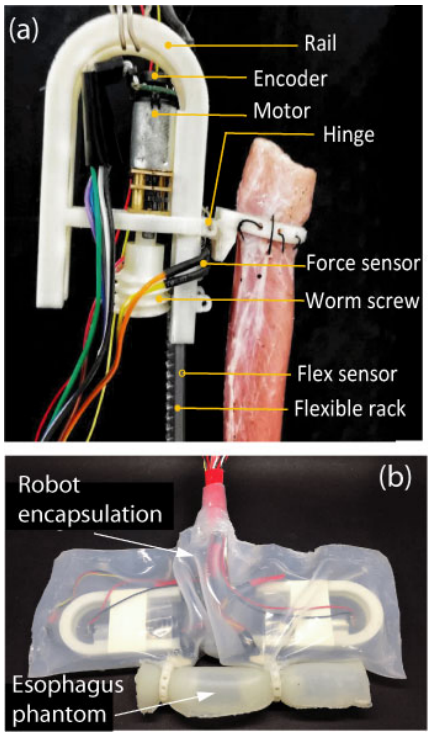

Fig. 2. Details of the SIR's parts. (a) inner components of the SIR as attached to a swine esophagus tissue, (b) implant encapsulated in an elastomeric sleeve.

45 g. With this design, the maximum usable rack length and tissue elongation ranges between 120 and 230 mm. The worm gears (Fig. 2 (a)) were 3D-printed using the Mojo Printer-Strastasys with an infill solid density of 100 and a layer height of 0.127 mm.

The tension force applied to the tissue by the implant is controlled via a proportional-integral (PI) controller. The controller varies the pulse width-modulated (PWM) voltage input of the gearmotor in order to maintain a desired output tension force in the tissue in the presence of output disturbances and measurement noise. An elastomeric sleeve made of Ecoflex 00-30 (Smooth-On, Inc.) is wrapped around the implant, as shown in Fig. 2 (b). The wrinkles in the elastomeric sleeve allow the full extension of the robot without opposing resistance. Through our experiments, we have used a phantom tubular tissue made of Ecoflex 00-30, as in Fig. 2 (b), to which the robot applies tension.

C. SIR Electrical Design

The electrical design is shown in Fig. 2 (a) and Fig. 3. A Baby Orangutan (Pololu) microcontroller was selected for this specific application because it provides two separate high-power motor drivers and is relatively small in size. Honeywell FSS1500NSR sensors were used to measure the force exerted against the tissue. These sensors provide low-amplitude signals that are conditioned by AD623 instrumentation amplifiers (Analog Devices), delivering a voltage gain of 22. The relative position of the implant was tracked using Pololu magnetic encoders to count the revolutions of the

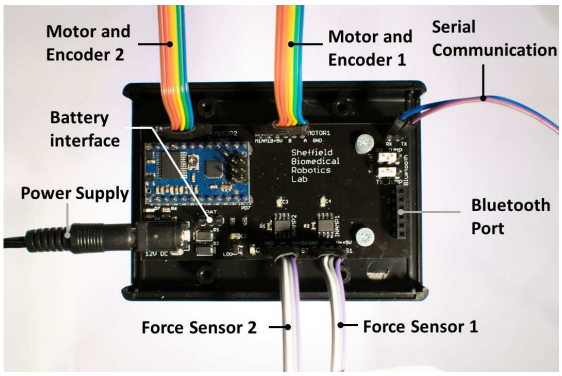

Fig. 3. Electronic circuit of the SIR.

298:1 DC motors. The flexion of the rack was monitored using a Spectra Symbol Flex 4.5 inch sensor. The flex sensor film was attached on the back of the rack. The system is designed so that it can be powered by either a 9-9.6V battery pack or an external, plug-in power supply.

IV. Shape-change Based Fault Tolerance Control

A. Force sensor fault detection and compensation

We implemented an autonomous fault tolerant scheme that exploits the robot's changes in shape (via bending) and size (via extension), as well as its unit redundancy (via symmetric design), in order to make the robot resilient to damage.

The fault diagnosis in this study was implemented only for the force sensor as a proof of concept of the proposed FTC. A comprehensive FTC will be the subject of our future work. We demonstrate two techniques to detect faults: out-of-boundary fault and force signal incongruency fault. The out-of-boundary fault refers to the force readings exceeding a range of expected operational values, potentially indicating control or sensor failures. Values exceeding the pre-defined range of 0.15N to 1.5N will trigger the out-of-boundary fault. The force signal incongruency fault refers to the two force sensors not having their readings positively correlated. When the robot is normally coupled to a tissue under tension it is expected that the two sensors will vary similarly, deferring by an offset; if not, a fault in one of the sensors is likely.

The fault compensation algorithm is triggered if a force fault is detected and attempts to mitigate the fault. A flow chart of the fault compensation algorithm is provided in Fig 4. We demonstrate four fault tolerance strategies that make use of the shape-changing and symmetric design of the robot, and which we refer to as retraction, recovery, deferral and halt strategy. If a fault is detected in the main force sensor (the force sensor in the main rail, which is active initially by default), the compensation scheme will retract the robot to a safe position using the main motor (retraction strategy) and the robot's diagnosis will be re-assessed. The safe position is defined as a fully retracted rack. In this position, the tension on the tissue is minimal, thus, safety is maximum. Starting from the safe position, the robot enters a recovery strategy by which it extends its rack

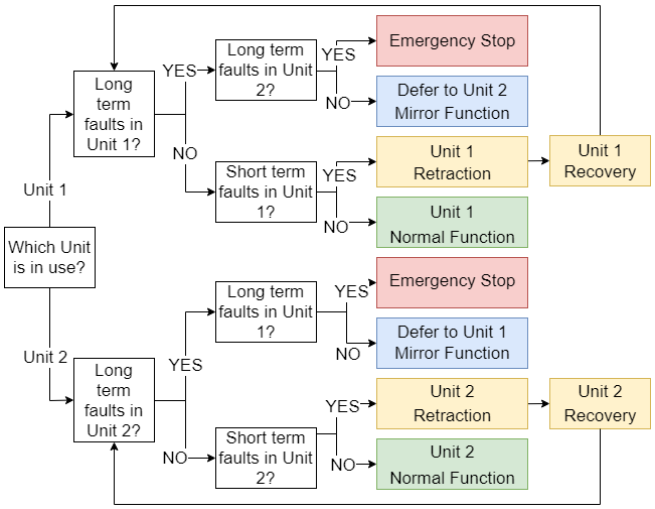

Fig. 4. Flowchart of the SIR's fault tolerant control.

in incremental steps to poll whether the fault is still present, thus classifying the fault as transient or permanent. If the sensor's reading recovers to expected values, it is classified as a transient fault, and the original control will be restored. However, if the force sensor fault persist or appears during the recovery phases, the SIR will enter in deferral strategy, by which the main unit is deactivated and the mirror unit is activated. When the system is deemed unfit for continued operation upon having applied all these strategies, the robot makes an emergency stop (halt strategy). The fault diagnosis and compensation scheme is tested in Section V.

B. Failure Mode and Effects Analysis (FMEA)

FMEA is a systematic tool used to identify potential problems, their impact and understanding how to overcome or mitigate them [21]. It is a bottom-up approach that focuses on the roots that could fail and it is rated based on three factors: Severity, Occurrence and Detection. A representative Design FMEA was performed at system level and the scope of this was limited to the force sensor. We analyzed the type of faults of the force sensor likely to occur and their severity. The force sensor failure is analyzed, identifying the failure modes, the effect of failure, as in Table I. Based on empirical trials, the failure modes associated with the force sensor were identified and their effects on the system were estimated. Three factors - Severity, Occurrence and Detection - were ranked from a range of 1 to 10. The Severity rating was estimated based on standard FMEA scale wherein a failure which could affect patient safety was given a ranking of 8 to 10. The Occurrence rating was estimated based on the number of times the faults occurred naturally during experiments. The Detection rating was estimated based on the system's ability to catch these faults when they occurred. The highest score of 1 was given for the Detection factor for the system that detected all faults. On multiplying these rankings, the initial Risk Priority Number (RPN_{ini}) was obtained and this has been documented in Table I. From Table I, it can be seen that the incongruity fault has the highest risk even after the implementation of corrective methods. Because of this, the demonstrations of the FTC implementation will be conducted on simulated incongruity faults.

V. Experiments and Results

A. Fault Detection and Retraction Reflex

We demonstrate the fault diagnosis of the force sensor and the retraction reflex of the SIR. The retraction reflex is a safety behavior by which the SIR will retract its rack to a safe position (no rack is exposed externally) to minimize potential hazardous impact on the tissue and start identifying the fault. Two experiments were performed to demonstrate the out-of-boundary and the force incongruency fault detection and the consequent retraction reflex. Feedback from the force sensor is the main control factor, as errors from this sensor may lead to unreasonable elongation forces that could damage the tissue. An abnormal situation would occur if the force sensor lost a reading or if a reading was unexpectedly large. When this type of out-of-boundary fault is confirmed the implant will retract to the safe position and the implant will be rediagnosed as in Section V-B.

Fig 5 (a) shows a fault in the main rail force sensor (FS1). The system was commanded to move from a starting force of $0.2\,\mathrm{N}$ to $0.4\,\mathrm{N}$; once it reached that point, a fault in FS1 was simulated by lifting the associated tissue attachment ring, thus making the sensor value drop ($90\,\mathrm{s}$). This fault was recognized as an out-of-boundary fault. Consequently, the system immediately retracts to a safe position as indicated by the encoder whose signal shows a displacement from 4 to $0\,\mathrm{mm}$. In a second experiment, we show the force incongruency fault. Fig 5 (b) shows a force reading fault in FS1. We simulated this fault by manually pressing on FS1. The initial force set point was $0.45\,\mathrm{N}$ and, once this was achieved, FS1 was pressed until a large difference was created between the two force sensors (70s). The system recognized the large difference as a force incongruency fault and retracted to safe position.

B. Robot Extension-enabled Active Recovery

Following the retraction reflex, the SIR will initiate an active operation to identify if the fault is transient or per-

TABLE I
FMEA

Failure	Effect	S	O	D	RPN	S	O	D	RPN	Reduced RPN
		Initial				After corrections				
Incongruent Readings	Tissue damage	9	5	6	270	9	5	1	45	83.3%
Out-of-boundary error	Pressure on tissue increases	8	4	6	192	8	4	1	32	83.3%

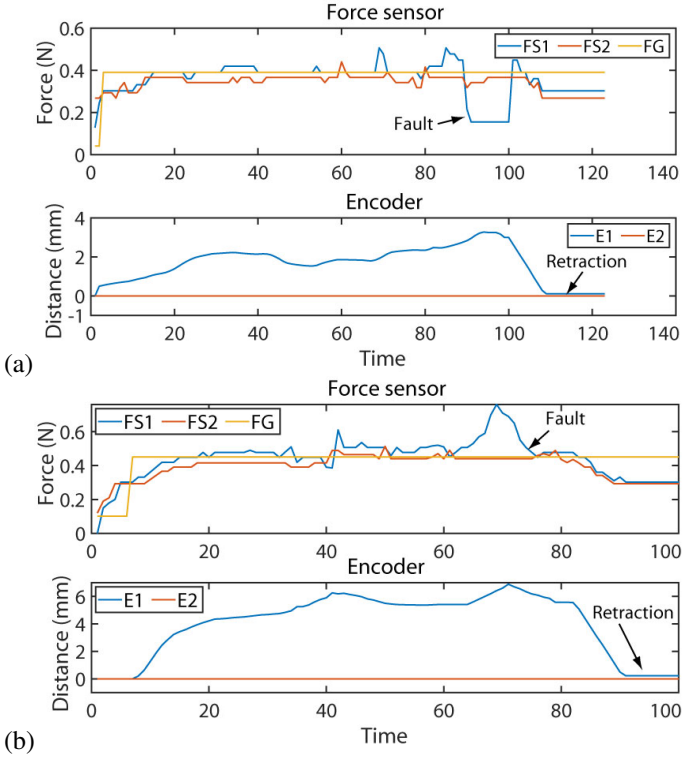

Fig. 5. Fault detection and retraction reflex: (a) out-of-boundary error, (b) incongruency error. FS1, E1 are main unit's force sensor and encoder, respectively. FS2, E2 are the mirror unit's force sensor and encoder, respectively. FG is the target force.

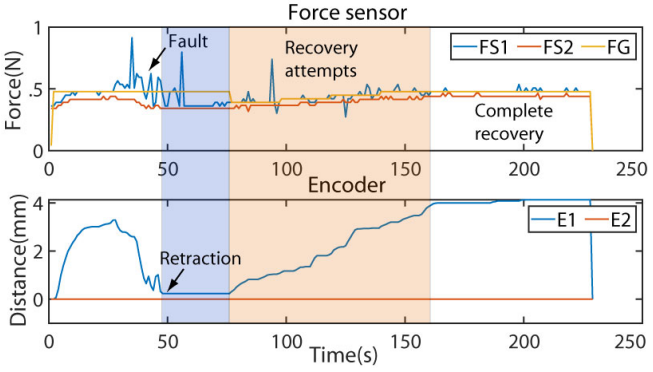

Fig. 6. Transient fault due to force readings incongruency, with successful recovery. Blue and orange shades stand for retraction and recovery attempts, respectively.

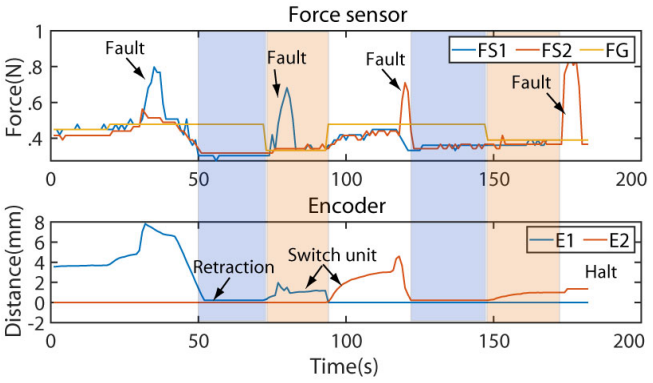

Fig. 7. Autonomous handling of transient and permanent faults, cycling through retraction, recovery, deferral and system halt. Blue and orange shades stand for retraction and recovery attempts, respectively.

manent. In this experiment, we demonstrate the automatic capability of the robot to handle a transient fault by evoking recovery as in Fig 6. The force sensor of the main rail (FS1) was pressed to create a surge in value which resulted in a high difference between the two force sensors (40s). The system determines this as a incongruency fault and retracts to a safe position which can be seen by the value of main rail encoder (E1) dropping to 0 mm. After 30 seconds in this mode, the system attempts to recover from the fault through four stages of recovery. These stages are set as four target forces, which are equidistantly determined within the original target force (before fault) and the force in the retraction state. Each recovery stage lasts 20 seconds. In each recovery stages, the robot extends its rack to increase the tension in the force sensors to poll if the fault persist. In this experiment, the fault is not present during the recovery and hence the robot classifies the fault as transient and returns to normal functioning with the main rail unit. The flex sensor readings varied between -1 and 1° during the experiment.

C. Redundancy-based Compensation

If a fault is recurrent the robot will classify it as a permanent fault, and switch the control to the robot's mirror unit. In this experiment, the main rail force sensor (FS1) was manually pressed to induce a fault as shown in Fig 7 (30s). The robot retracts to safe position as seen from the encoder value dropping to zero (50s). During recovery stage 1, FS1 was pressed again which can be seen by the surge in value (80s). If a fault persists or returns during the recovery then it gets registered as a permanent fault. Consequently, the control switches over to the mirror unit. This switching can be observed from the main unit's encoder value (E1) dropping to zero and the mirror unit's encoder value (E2) increasing. The mirror unit's force sensor (FS2) was manually pressed to generate a transient fault (120s) and the system retracts to safe position as seen from E2 signal dropping to zero. The system attempts a recovery during which this fault was induced again (170s). This becomes a permanent fault and when both units have permanent faults, the system goes to an emergency stop (motors' power is disabled). During this experiment, the flex sensor readings varied between -2 and 2°.

D. Flexion-enabled Fault Identification and Disambiguation

Due to the robot's flexibility and its coupling with the viscuoelastic tissue, there is a strong correlation between the robot's rack bending and tissue tension. When tension is applied to the tissue, the robot will flex, and when the tissue is relaxed (as a result of tissue viscuoelastic relaxation or growth), the robot will straighten. This correlation can be used to diagnose faults in force, bending sensing or structural damage in the rack. Furthermore, this correlation can be used to disambiguate which of the force sensors are faulty,

as shown in Fig 8. In contrast, in stiff technology, such as aircraft, the typical methodology is to use three identical sensors in order to remove ambiguity in identifying the fault. The correlation coefficient is calculated using the following formula:

$$C_1 = \frac{\sum_{i=1}^{n}(FS1_i - \mu_{FS1})(FS2_i - \mu_{FS2})}{\sqrt{\sum_{i=1}^{n}(FS1_i - \mu_{FS1})^2}\sqrt{\sum_{i=1}^{n}(FS2_i - \mu_{FS2})^2}} \quad (1)$$

In equation (1), C_1 is the correlation coefficient of variables FS1 and FS2. μ is the mean value of the variables. Similarly the formula is applied to obtain the correlation coefficient of the other two pairs of variables.

The aim of this experiment is to demonstrate how the correlation coefficient can be used to identify which force sensor is faulty. Once the SIR was online, FS1 was manually pressed to induce an incongruency fault as shown in Fig 8 (65s). On observing the correlation coefficient, it can be seen that prior to pressing on FS1 the coefficients had a high positive correlation. But, the surge in FS1 causes the coefficients associated with it to drop down to nearly zero. This signifies that there is no meaningful correlation and this drop in correlation is used to identify that FS1 is faulty. The system consequently retracts to a safe position as seen from the encoder values dropping to zero at 80s.

E. Post Shape-changing based FTC FMEA

The FMEA risk analysis was performed again after taking into account the corrective measures we implemented in the shape-changing robot, that is, the retraction, recovery, deferral and halt. The failure effects were estimated empirically, the S, O and R factors were ranked and the RPN (RPN_{cor}) was calculated again (Table I). Comparing to the initial RPN (RPN_{ini}), the reduced risk percentage was calculated as:

$$\text{Reduced Risk}\,(\%) = ((RPN_{ini} - RPN_{cor})/RPN_{ini}) \times 100. \quad (2)$$

The results, presented in Table I, show that the shape-changing FTC reduced the fault risks by at least 83% for the first and last fault specified in the Table, which are particularly investigated in this study.

VI. Discussions and Conclusion

We introduced a fault-tolerant control in a shape-changing robot and demonstrated the key advantages for the robotic self-maintenance, which is critically relevant to implantable technology that is expected to function over long-term periods and in challenging biological environments. The shape-changing design plays a critical role in the robot's fault tolerant operation. First, its flexibility and extendability diminish robot's self-damage by conforming to the dynamic environment inside the body by changing shape or size, respectively. This characteristic is discussed in [20]. Furthermore, the flexibility of the robot allows the disambiguity in fault identification. Using retraction/extension, the robot is endowed with reflexes and behaviors to ensure safety when damaged, and polling for re-diagnosing faults. The

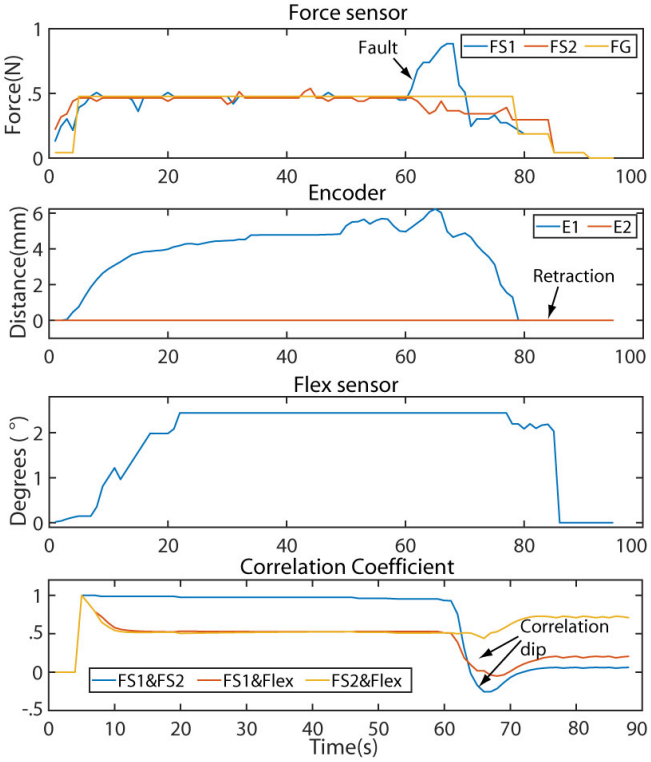

Fig. 8. Correlation between the two force sensors and the flex sensor, as an indicator of incongruency fault in the main force sensor (FS1).

symmetric design of the robot enables redundant-based fault compensation control. We demonstrated initial results of the implant overcoming transient and permanent and we show a reduction of the fault risks by at least 83%. In the current study, we limited the investigation to force sensor faults. Future work will be focused on the development of a comprehensive fault-tolerant framework including mechanical recovery. The final validation of this study is planned in survival tests with large animals. A stiff implant would not comply with body motions and thus cause irritation on the biological tissue and induce intense foreign body reaction [22]. In this case, the SIR maintains the force on the tissue by extending or retracting in accordance with the body motion and stretching of tissue.

This study shows the advantages of safety-critical robots to feature shape-changing features, such as flexion and extension. First, similar to a muscle, a robot endowed with such features can use its motion to diagnose faults (e.g., via flexion, extension) or treat them (e.g., via retraction). Second, by combining proprioceptive sensing (e.g., flex sensor) and exteroceptive sensing (e.g., force sensor), the identification of active redundant sensors (e.g., the two sensors) fault is more efficient and unambiguous.

Acknowledgement

We thank Daniel Diaz, Sarunas Nejus for their help in the development of this platform, and Mohamed Atwya for valuable inputs.

REFERENCES

[1] S. Eming, T. Wynn, and P. Martin, "Inflammation and metabolism in tissue repair and regeneration," *Science*, vol. 356, pp. 1026–1030, 2017.

[2] J. E. Foker, B. C. Linden, E. M. Boyle, and C. Marquardt, "Development of a true primary repair for the full spectrum of esophageal atresia." *Annals of surgery*, vol. 226, no. 4, pp. 533–41; discussion 541–3, oct 1997.

[3] A. U. Spencer, X. Sun, M. El-Sawaf, E. Q. Haxhija, D. Brei, J. Luntz, H. Yang, and D. H. Teitelbaum, "Enterogenesis in a clinically feasible model of mechanical small-bowel lengthening," *Surgery*, vol. 140, no. 2, pp. 212–220, 2006.

[4] C. Angeli and A. Chatzinikolaou, "On-line fault detection techniques for technical systems: A survey." *International Journal of Computer Science and Applications*, vol. 1, no. 1, pp. 12–30, 2004.

[5] P. Moshayedi, G. Ng, J. Kwok, G. Yeo, C. Bryant, J. Fawcett, K. Franze, and J. Guck, "The relationship between glial cell mechanosensitivity and foreign body reactions in the central nervous system." *Biomaterials*, vol. 35, no. 13, pp. 3919–25, 2014.

[6] W. A. Gray, A. Feiring, M. Cioppi, R. Hibbard, B. Gray, Y. Khatib, D. Jessup, W. Bachinsky, E. Rivera, J. Tauth, R. Patarca, J. Massaro, H. P. Stoll, and M. R. Jaff, "S.M.A.R.T. self-expanding nitinol stent for the treatment of atherosclerotic lesions in the superficial femoral artery (STROLL): 1-year outcomes," *Journal of Vascular and Interventional Radiology*, vol. 26, no. 1, pp. 21–28, 2015.

[7] L. Xu, S. R. Gutbrod, A. P. Bonifas, Y. Su, M. S. Sulkin, N. Lu, H.-J. Chung, K.-I. Jang, Z. Liu, M. Ying, C. Lu, R. C. Webb, J.-S. Kim, J. I. Laughner, H. Cheng, Y. Liu, A. Ameen, J.-W. Jeong, G.-T. Kim, Y. Huang, I. R. Efimov, and J. a. Rogers, "3D multifunctional integumentary membranes for spatiotemporal cardiac measurements and stimulation across the entire epicardium." *Nature communications*, vol. 5, p. 3329, 2014.

[8] E. T. Roche, M. A. Horvath, I. Wamala, A. Alazmani, S.-E. Song, W. Whyte, Z. Machaidze, C. J. Payne, J. C. Weaver, G. Fishbein, J. Kuebler, N. V. Vasilyev, D. J. Mooney, F. A. Pigula, and C. J. Walsh, "Soft robotic sleeve supports heart function." *Science Translational Medicine*, vol. 9, no. 373, pp. 1–12, 2017.

[9] S. Miyashita, S. Guitron, K. Yoshida, S. Li, D. D. Damian, and D. Rus, "Ingestible, controllable, and degradable origami robot for patching stomach wounds," *Proceedings - IEEE International Conference on Robotics and Automation*, vol. 2016-June, no. 4, pp. 909–916, 2016.

[10] D. D. Damian, S. Arabagi, P. E. Dupont, A. Fabozzo, P. Ngo, R. Jennings, M. Manfredi, and P. E. Dupont, "Design of a Robotic Implant for in-vivo Esophageal Tissue Growth," *Proceedings - IEEE International Conference on Robotics and Automation*, no. 1, pp. 73–74, 2014.

[11] E. R. Perez-Guagnelli, S. Nejus, J. Yu, S. Miyashita, Y. Liu, and D. D. Damian, "Axially and radially expandable modular helical soft actuator for robotic implantables," in *Proceedings of 2018 IEEE International Conference on Robotics and Automation*. IEEE, 2018, pp. 4297–4304.

[12] D. D. Damian, K. Price, S. Arabagi, I. Berra, Z. Machaidze, S. Manjila, S. Shimada, A. Fabozzo, G. Arnal, D. V. Story, J. D. Goldsmith, A. T. Agoston, C. Kim, R. W. Jennings, P. D. Ngo, M. Manfredi, and P. E. Dupont, "In vivo tissue regeneration with robotic implants." *Science Robotics*, vol. 3, no. 14, p. eaaq0018, 2018.

[13] K. Cleary and C. Nguyen, "State of the art in surgical robotics: Clinical applications and technology challenges," *Computer Aided Surgery*, vol. 6, no. 6, pp. 312–328, 2001.

[14] N. J. Dowler, "Applying software dependability principles to medical robotics," *Computing Control Engineering Journal*, vol. 6, no. 5, pp. 222–225, Oct 1995.

[15] M.L.Visinsky, J.R.Cavallaro, and I.D.Walker, "Robotic fault detection and fault tolerance: A survey," *Reliability Engineering & System Safety*, vol. 46, pp. 139–158, 1994.

[16] J. Bongard, V. Zykov, and H. Lipson, "Resilient machines through continuous self-modeling," *Science*, vol. 314, pp. 1118–1121, 2006.

[17] M. T. Tolley, R. F. Shepherd, B. Mosadegh, K. C. Galloway, M. Wehner, M. Karpelson, R. J. Wood, and G. M. Whitesides, "A resilient, untethered soft robot," *Soft Robotics*, vol. 1, pp. 213–223, 2014.

[18] A. Cully, J. Clune, D. Tarapore, and J.-B. Mouret, "Robots that can adapt like animals," *Nature*, vol. 521, pp. 503–507, 2015.

[19] K.-J. Kim and S.-B. Cho, "Automated synthesis of multiple analog circuits using evolutionary computation for redundancy-based fault-tolerance," *Applied Soft Computing*, vol. 12, no. 4, pp. 1309–1321, 2012.

[20] M. Atwya, C. Kavak, E. Alisse, Y. Liu, and D. D. Damian, "A flexible and expandable robot for tissue-regenerative therapies," 2020, (under review).

[21] Y. Maddahi, A. Maddahi, S. Mohammad, and H. Monsef, "Design improvement of wheeled mobile robots: Theory and experiment," *World Applied Sciences Journal*, vol. 16, pp. 263–274, 01 2012.

[22] J. Subbaroyan, D. C. Martin, and D. R. Kipke, "A finite-element model of the mechanical effects of implantable microelectrodes in the cerebral cortex," *Journal of Neural Engineering*, vol. 2, no. 4, p. 103–113, Nov 2005.